Magnon modes and magnon-vortex scattering in two-dimensional easy-plane ferromagnets

B. A. Ivanov,* H. J. Schnitzer, and F. G. Mertens
Physikalisches Institut, Universität Bayreuth, D-95440 Bayreuth, Germany

G. M. Wysin
Department of Physics, Kansas State University, Cardwell Hall, Manhattan, Kansas 66506
(Received 9 October 1997; revised manuscript received 11 May 1998)

We calculate the magnon modes in the presence of a vortex on a circular system, combining analytical calculations in the continuum limit with a numerical diagonalization of the discrete system. The magnon modes are expressed by the S matrix for magnon-vortex scattering, as a function of the parameters and the size of the system and for different boundary conditions. Certain quasilocal translational modes are identified with the frequencies which appear in the trajectory $\vec{X}(t)$ of the vortex center in recent molecular dynamics simulations of the full many-spin model. Using these quasilocal modes we calculate the two parameters of a third-order equation of motion for $\vec{X}(t)$. This equation was recently derived by a collective variable theory and describes very well the trajectories observed in the simulations. Both parameters, the vortex mass and the factor in front of $\dddot{\vec{X}}$, depend strongly on the boundary conditions. [S0163-1829(98)07937-5]

I. INTRODUCTION

Two-dimensional (2D) magnets have been intensively investigated due to different reasons: There are several classes of quasi-2D materials for which the magnetic interactions within planes of magnetic ions are typically three to six orders of magnitude larger than the interactions between the planes. These classes include layered magnets (e.g., Rb_2CrCl_4), graphite intercalated compounds (e.g., $CoCl_2$), magnetic lipid layers (e.g., manganese stearate), and high-T_c superconductors. For theoreticians 2D magnets with XY- or easy-plane symmetry are particularly interesting due to the existence of vortices, which have nontrivial properties from the viewpoint of certain homotopical groups, see Refs. 1–3.

There are two types of vortices: In-plane (IP) ones with all spins lying in the easy plane and out-of-plane (OP) ones having nonzero spin components orthogonal to the easy plane. Both types have a π_1-topological charge or vorticity $q = \pm 1, \pm 2, \ldots$, which determines the directions of the spins in the easy plane far away from the vortex center. The OP vortices have an additional π_2-topological charge (Pontryagin invariant, see Ref. 3) $Q = -\frac{1}{2}qp$, where p is integer. p is denoted polarization because its sign determines to which side of the easy plane the spins point in the vortex center. Therefore the IP vortices can be considered as having $p = 0$. For $Q \neq 0$ there is a gyrocoupling force, or gyroforce, which is formally equivalent to the Lorentz force.[4]

Besides the vortices, which are strongly nonlinear excitations, there are also magnons. The dynamic properties of 2D easy-plane magnets can be described by a phenomenological theory which assumes two ideal gases for the vortices and magnons.[5] The vortex-magnon interaction naturally is the next question which arises. In particular, one would like to know how the dynamics of the vortices is affected by this interaction.

For 1D magnets the soliton-magnon interaction is nearly reflectionless. In this case the main effect of the soliton-magnon interaction is the change of the magnon density of states, which affects strongly the soliton density in thermal equilibrium.[6] For 2D magnets the vortex density can be obtained from the correlation length by a renormalization group approach,[7–9] therefore the vortex-magnon interaction is not so important for the density. In principle, it can be important for the damping force which acts on a vortex (or soliton) in a near-equilibrium magnon gas.[2] On the other hand, the damping force for the 2D case can be obtained by general hydrodynamic theories for the relaxation processes in magnets.[10]

The most important effect of the vortex-magnon interaction seems to be that for a finite system certain magnon modes are excited due to the vortex motion, and vice versa. Such modes were obtained in recent papers[11–13] by a numerical diagonalization for relatively small, circular, discrete systems. A calculation in the continuum limit was presented for the antiferromagnetic case.[13] Analytical investigations were done for planar vortices in antiferromagnets[14] and ferromagnets.[15] These articles demonstrate nontrivial properties of the eigenmodes, e.g., the presence of quasilocal[11,12] or truly local[13] modes. Moreover, the relevance of these modes for the vortex dynamics was shown, in particular an IP-OP transition was predicted[11,12] and an effective vortex mass was defined and calculated using the above modes.[16] However, for OP vortices all this was based on the numerical diagonalization of small systems with fixed (Dirichlet) boundary conditions (BC's).

This article deals with a more general theory of vortex-magnon coupling for arbitrarily large systems with circular symmetry and general boundary conditions. The method consists of a natural combination of analytical calculations in the continuum limit with numerical diagonalization of discrete systems. The main issue is the calculation of the scattering matrix for vortex-magnon collisions. (For antiferromagnets this matrix was calculated by a different method.[13]) Using these data general formulas for the eigenfrequencies

are obtained, as a function of the parameters and size of the system, and for different boundary conditions.

An important point is a link with a recent collective variable theory[17] in which an equation of motion was derived which describes very well the vortex trajectories observed in computer simulations. This equation is third order in time, and is a generalization of the Thiele equation[18,19] which is first order in time. Using the scattering data the parameters of the third-order equation of motion can be calculated, and agree very well with those obtained from simulations.[17]

II. THE MODEL AND ELEMENTARY EXCITATIONS

We consider the classical 2D model of a Heisenberg ferromagnet (FM) with the Hamiltonian

$$\hat{H} = -J \sum_{(\vec{n},\vec{n}')} [\vec{S}_{\vec{n}}\vec{S}_{\vec{n}'} - (1-\lambda)S_{\vec{n}}^z S_{\vec{n}'}^z]. \qquad (1)$$

Here $J > 0$ is the exchange integral and $0 \leq \lambda < 1$ describes easy-plane anisotropy. The spins $\vec{S}$ are classical vectors on a square lattice with the lattice constant a_0. $\vec{n}, \vec{n}'$ denote nearest-neighbor lattice sites. Our main interest lies in the small anisotropy case which corresponds to $1 - \lambda \ll 1$.

A continuum model for FM's can be derived from Eq. (1) in the usual way defining the unit vector of magnetization as a function of continuous variables $\vec{r}$ and t, i.e., $\vec{m}(\vec{r},t) = \vec{S}_{\vec{n}}(t)/S$. The dynamical equations for $\vec{m}$ have the form of the well-known Landau-Lifshitz equation, see Refs. 1, 2. In usual angular variables $[m_x + im_y = \sin\theta \exp(i\phi), m_z = \cos\theta]$ they can be written as

$$\nabla^2\theta - \sin\theta\cos\theta\left[(\nabla\phi)^2 - \frac{1}{r_v^2}\right] = +\frac{\sin\theta}{cr_v}\frac{\partial\phi}{\partial t}, \qquad (2)$$

$$\nabla(\sin^2\theta\nabla\phi) = -\frac{\sin\theta}{cr_v}\frac{\partial\theta}{\partial t}, \qquad (3)$$

where r_v and c are the characteristic length scale and magnon speed, respectively. For the Hamiltonian (1), we have

$$r_v = \frac{a_0}{2}\sqrt{\frac{\lambda}{1-\lambda}}, \quad c = 2JSa_0\sqrt{1-\lambda}, \qquad (4)$$

where we set $\hbar = 1$. Note that the Eqs. (2), (3) arise in the long-wave approximation $(a_0|\nabla\vec{m}| \ll 1)$ not only for the model we are considering here, but for a whole set of discrete models, for example, FM's on different kinds of lattices and FM's with additional single-ion anisotropy. Merely the expressions for c and r_v change. For the homogeneous ground state (all spins are parallel and confined to the easy plane) the 2D model has well-known magnon excitations with the gapless dispersion law

$$\omega = ck(1 + k^2 r_v^2)^{1/2}, \qquad (5)$$

where $k = |\vec{k}|$ and $\vec{k}$ is the magnon wave vector.

Other well-known excitations are the OP vortices, described by the formulas

$$\theta = \theta_0(r), \quad \phi = q\chi + \varphi_0, \qquad (6)$$

where r and χ are polar coordinates and φ_0 is an arbitrary constant. The function θ_0 is the solution of a nonlinear ordinary differential equation which cannot be solved analytically.[1,2] Numerical integration, however, shows a surprisingly good agreement with the data obtained from the numerical analysis of the full discrete model (1), even for $r_v = 1.5a_0$ ($\lambda = 0.9$), Ref. 13. This means that at least concerning static properties strong inequalities such as $a_0|\nabla\vec{m}| \ll 1$ can be replaced by usual ones. As will be seen, the same is correct for some dynamical properties, too. θ_0 fulfills the boundary conditions $\cos\theta_0 \to p$ for $r \to 0$ and $\theta_0 \to \pi/2$ for $r \to \infty$. q and p are topological charges of vorticity and polarization. In the following OP vortices with $q = 1$ will be considered; for definiteness we set $p = 1$.

III. NORMAL MODES ON THE VORTEX: CONTINUUM APPROACH

We consider small deviations from the static vortex solutions, i.e.,

$$\theta = \theta_0(r) + \vartheta, \quad \phi = q\chi + (\sin\theta_0)^{-1}\mu. \qquad (7)$$

Substituting this in Eqs. (2) and (3) and linearizing in ϑ and μ gives the following set of coupled partial differential equations:

$$[-\nabla_x^2 + V_1(x)]\vartheta + \frac{2q\cos\theta_0}{x^2}\frac{\partial\mu}{\partial\chi} = -\frac{r_v}{c}\frac{\partial\mu}{\partial t}, \qquad (8)$$

$$[-\nabla_x^2 + V_2(x)]\mu - \frac{2q\cos\theta_0}{x^2}\frac{\partial\vartheta}{\partial\chi} = +\frac{r_v}{c}\frac{\partial\vartheta}{\partial t}, \qquad (9)$$

where $x = r/r_v$ and $\nabla_x = r_v\nabla$. The additional factor $(\sin\theta_0)^{-1}$ in Eq. (7) was introduced for convenience, because it leads to equations that are symmetric in ϑ and μ with Schrödinger-type differential operators in front. The ''potentials'' $V_1(x)$, $V_2(x)$ have the same form as for the antiferromagnet,[13]

$$V_1 = \left[\frac{q^2}{x^2} - 1\right]\cos 2\theta_0, \quad V_2 = \left[\frac{q^2}{x^2} - 1\right]\cos^2\theta_0 - \left[\frac{d\theta_0}{dx}\right]^2, \qquad (10)$$

but the dynamical parts differ strongly.

In order to solve Eqs. (8), (9) the following ansatz for ϑ and μ is appropriate:

$$\vartheta = \sum_n \sum_{m=-\infty}^{+\infty} \{[f_\alpha' + if_\alpha'']\exp(im\chi + i\omega_\alpha t) + \text{c.c.}\}, \qquad (11)$$

$$\mu = \sum_n \sum_{m=-\infty}^{+\infty} \{[g_\alpha' + ig_\alpha'']\exp(im\chi + i\omega_\alpha t) + \text{c.c.}\}. \qquad (12)$$

$\alpha = (n,m)$ is a full set of numbers labeling the magnon eigenstates. Substituting this ansatz gives two uncoupled sets of two equations for the pairs of functions (f',g'') on the one side and (f'',g') on the other side. However, the equations for (f'',g') can be obtained from the corresponding equations for (f',g'') simply by replacing $m \to -m$ and $\omega \to$

$-\omega$. Thus, among the four functions f', f'', g', and g'' only two are independent. Therefore, instead of Eqs. (11),(12) we can use the simplified ansatz

$$\vartheta = \sum_n \sum_{m=-\infty}^{+\infty} f_\alpha(r)\cos(m\chi + \omega_\alpha t + \delta_m), \qquad (13)$$

$$\mu = \sum_n \sum_{m=-\infty}^{+\infty} g_\alpha(r)\sin(m\chi + \omega_\alpha t + \delta_m), \qquad (14)$$

with arbitrary phases δ_m. For the functions f and g (the index α is omitted in the following) we then finally obtain the following two differential equations:

$$\left[\frac{d^2}{dx^2} + \frac{1}{x}\frac{d}{dx} - \frac{m^2}{x^2} - V_1\right]f = \left[\frac{\omega r_v}{c} + \frac{2qm\,\cos\,\theta_0}{x^2}\right]g, \qquad (15)$$

$$\left[\frac{d^2}{dx^2} + \frac{1}{x}\frac{d}{dx} - \frac{m^2}{x^2} - V_2\right]g = \left[\frac{\omega r_v}{c} + \frac{2qm\,\cos\,\theta_0}{x^2}\right]f. \qquad (16)$$

f and g cannot be determined analytically from Eqs. (15), (16). The ''potentials'' $V_1(x)$ and $V_2(x)$ in these equations are not small, and the use of the Born approximation looks inadequate; for IP vortices and $m=0,\pm 1$ this was already mentioned in Ref. 15. Only the asymptotic behavior can be calculated. For $r\to 0$ we obtain $g,f\sim r^{|q+m|}$, which describes the presence of a ''hole'' in the functions ϑ, μ at the vortex core for large values of m (see Sec. IV). Only the case $|m|=1$ can be considered in a long-wave approximation, see below, Eqs. (22)–(27).

For the IP vortex, where $\cos\,\theta_0$ is zero, the modes corresponding to $\pm|m|$ are degenerate. As a change of sign in the number m can also be interpreted as a change of the sense of rotation of the eigenmode (change of sign in the eigenfrequency ω), physically we have the situation of two independent oscillators rotating clockwise and counterclockwise with the same frequency (which can also be combined to give two linear oscillators in independent directions).

For the OP vortex, however, with $\cos\,\theta_0\neq 0$, this degeneracy is removed due to the presence of the term with $2qm\,\cos\,\theta_0/r^2$. Therefore the two senses of rotations corresponding to positive and negative frequencies are not equivalent anymore. The presence of this term is also responsible for the fact that the Eqs. (15) and (16) are only invariant under the combined conjugation of both topological charges $(q,p)\to(-q,-p)$. The product qp is proportional to the magnitude of the so-called gyrovector, which acts on the vortex as a (self-induced) magnetic field in the z direction for a charged particle. Therefore, physically, for $|m|\geqslant 1$ the removal of the $\pm|m|$ degeneracy in the OP case can be understood as the effect of a gyroscopic force.

In order to describe the magnon scattering due to the vortex, we note that without the vortex the eigenvalue problem (EVP), Eqs. (8), (9) can be reduced to a usual Schrödinger EVP (SEVP) with the general solution

$$\mu = \sum_m C_m J_m(kr)\sin(m\chi + \omega t + \delta_m), \qquad (17)$$

$$\vartheta = \sum_m C_m \frac{kr_v}{\sqrt{1+k^2r_v^2}}J_m(kr)\cos(m\chi + \omega t + \delta_m). \quad (18)$$

The J_m are Bessel functions, k and ω are connected by the dispersion law (5), and C_m and δ_m are arbitrary constants. For a finite circular system with radius L and general boundary conditions

$$\left(a\mu + br_v\frac{\partial\mu}{\partial r}\right)_{r=L} = 0, \quad \left(a\vartheta + br_v\frac{\partial\vartheta}{\partial r}\right)_{r=L} = 0, \quad (19)$$

with arbitrary constants a and b; the values of the frequencies ω are determined by the roots of linear combinations of Bessel functions and its derivatives. Note that *all* frequencies for the system without a vortex have a $1/L$ dependence with respect to the system size. For free boundary conditions, i.e., $a=0$ in Eq. (19), there is a Goldstone mode (GM) with $\omega=0$ due to the rotational symmetry in spin space of the model. For $a\neq 0$ this symmetry is obviously broken.

In the presence of a vortex, one can use the approximate formula $f\approx kr_vg/(1+k^2r_v^2)^{1/2}$ for large distances $r\gg r_v$ and then the EVP (15), (16) reduces to the form of a SEVP, too. The solutions have the same form as Eqs. (17), (18); one only has to replace

$$J_m(kr)\to J_m(kr) + \sigma_m(k)Y_m(kr). \qquad (20)$$

Here the Y_m are Neumann functions. The quantity $\sigma_m(k)$ determines the intensity of magnon scattering due to the presence of the vortex. In usual scattering theory for 2D Schrödinger equations the S matrix $S_m(k)$ can be represented as

$$S_m(k) = \frac{1-i\sigma_m(k)}{1+i\sigma_m(k)}. \qquad (21)$$

The values of $\sigma_m(k)$ are determined by the shape of the solution near the vortex core, practically at $r/r_v<3\cdots 4$. Due to the structure of the continuum equations (15), (16), $\sigma_m(k)$ must be some universal function of $\kappa=kr_v$, independent of the concrete values of the magnetic coupling constants, the system size or the applied boundary conditions.

$\sigma_m(k)$ could be calculated directly by solving the set of equations (15), (16) using a shooting procedure as described in Ref. 13 for the case of the antiferromagnet. The shooting parameter is the free constant which appears in the general solution of the set of two coupled Schrödinger-like EVP's. In this article we used another approach and extracted the scattering data from the eigenfrequencies ω_i we found numerically for the discrete 2D system in Sec. IV.

In the next section the general properties of $\sigma_m(k)$ will be established for different m, and characteristic features of the normal modes will be discussed. Here we consider only the case $|m|=1$, for which the S matrix in the long-wave approximation can be calculated analytically.

This can be done by using the fact that for $k=0$ ($\omega=0$) and $L\to\infty$ a nontrivial solution of Eqs. (15), (16) is known, and by applying a special perturbation theory. This solution reads $f_0=d\theta_0/dx$, $g_0=-\sin\,\theta_0/x$, and corresponds to a vortex displacement (translational Goldstone mode).

In order to construct the asymptotics of such a solution for a small but finite frequency, we make the ansatz

$$f = (d\theta_0/dx)[1+\alpha(x)], \quad g = -(\sin \theta_0/x)[1+\beta(x)], \tag{22}$$

where $\alpha(x), \beta(x)$ must be proportional to ω. Inserting this ansatz into the set of Eqs. (15), (16), multiplying Eq. (16) with g_0 and Eq. (15) with f_0, and adding the results, one obtains the equation

$$\left\{\left[\beta'\left(\frac{\sin \theta_0}{x}\right)^2 + \alpha'(\theta_0')^2\right]x\right\}' = 2\frac{\omega r_v}{c}(\cos \theta_0)'. \tag{23}$$

Here the prime denotes d/dx, and small terms such as $\omega\alpha$, $\omega\beta$ were omitted. The formal solution of this equation can be written as

$$\beta(x) = \beta(0) - \int_0^x \alpha'(x)(x\theta_0'/\sin \theta_0)^2 dx$$
$$- (\omega r_v/c)\int_0^x [x/\cos^2(\theta_0/2)]dx. \tag{24}$$

It is easy to see that the last term is divergent for $x\to 0$, while the integral with $\alpha'(x)$ is convergent due to the presence of $\theta'(x) \sim \exp(-x)$. Thus, far from the vortex core we simply have

$$\beta(x) \simeq -(\omega r_v/c)x^2 = -kr_v x^2, \tag{25}$$

valid in the region $1 \ll x \ll (1/kr_v)^{1/2}$. $g(r)$ then reads

$$g(r) \simeq \frac{r_v}{r} - kr_v\left(\frac{r}{r_v}\right). \tag{26}$$

On the other hand, in the region $r_v \ll r \ll (r_v/k)^{1/2}$ the arguments of the Bessel functions in (20) are small: $kr \ll (kr_v)^{1/2} \ll 1$. Using the asymptotics $J_1(kr) = kr/2$, $Y_1(kr) = -2/\pi kr$, one can rewrite Eq. (26) in the form

$$g(r) \simeq \text{const}\left\{\frac{kr}{2} + \frac{\pi kr_v}{4}\left(-\frac{2}{\pi kr}\right)\right\}$$
$$\sim J_1(kr) + \frac{\pi kr_v}{4}Y_1(kr), \tag{27}$$

which gives us the long-wave approximation of the scattering amplitude: $\sigma_{\mp 1} \to \pm \pi kr_v/4$. This is in good agreement with the numerical data as we will see in the next section.

IV. NUMERICAL DIAGONALIZATION AND SCATTERING DATA CALCULATION

A numerical diagonalization of the same model we are considering here was also already performed by Wysin and Völkel.[12] These authors found, for example, the splitting of the $m \neq 0$ modes for OP vortices, as discussed above, and the lack of such a splitting for IP vortices. For a detailed description of the eigenvalues and eigenfunctions of Eq. (1) we therefore refer to their paper. For the rest of this section we relate some points which were not discussed in Ref. 12 including a short description of discreteness effects. Our main interest however, lies in the scattering of magnons due to the presence of a vortex.

We consider a circular system of radius L on a square lattice with either fixed (Dirichlet) or free (Neumann) bound-

ary conditions. Static vortex solutions were obtained using a relaxation procedure similar to that described in Ref. 12, or, in slightly more detail, in Ref. 20.

One problem with the diagonalization of 2D systems is that the number of sites in the system and therefore the dimension of the matrix to diagonalize grows very rapidly with the linear size of the system. Already for a rather small system with radius $L = 20a_0$ this matrix has dimension 2528×2528. If we use a conventional numerical method which needs to store the whole matrix in the memory of the computer, this is already more or less the size limit for matrices which can practically be diagonalized. In order to go further, we applied a special method which takes advantage of the structure and sparseness of the matrix. Details are described in the Appendix. Using this method we calculated the lowest eigenvalues and eigenvectors for systems up to $L/a_0 = 100$ corresponding to a matrix with dimensions 62856×62856.

The eigenvalue spectrum we obtained for fixed boundary conditions is plotted in Fig. 1 as a function of the anisotropy parameter λ for different values of the angular momentum quantum number $|m|$. For comparison, we have also calculated the eigenvalues for a system linearized around the ferromagnetic ground state of the model (i.e., *without* a vortex being present in the system). These data are the dashed lines in Fig. 1. $\lambda_c \approx 0.70$ is the critical value of anisotropy which separates the different regimes of stability of IP and OP vortices. As can easily be seen, the mode which is responsible for this transition is the $m = 0$ mode (the lowest branch in Fig. 1), which becomes soft at λ_c. Mainly the $m = 0$ and $|m| = 1$ modes are sensitive to the IP-OP transition. The eigenvalues above λ_c are split where for fixed boundary conditions the lower branch corresponds to negative m and the upper branch to positive m.

For $\lambda < \lambda_c$, only eigenmodes with *odd* $|m|$ are twofold degenerate, as predicted in the continuum theory. For *even* $|m|$ the expected degeneracy is slightly removed. This is a discreteness effect, due to the fourfold symmetry of the underlying square lattice: eigenvectors with even $|m|$ tend on the one hand to align with a coordinate system parallel to the symmetry axes of the underlying lattice, and on the other hand with a coordinate system parallel to the lattice diagonals. The latter eigenmodes oscillate with a slightly higher frequency.

The classification of the eigenvalues according to values of $|m|$ was done by expanding the eigenvectors in a Fourier series similar to Eqs. (13), (14) (excluding the time-dependent part). For $\lambda = 0.9$ some of the radial profiles of eigenvectors obtained this way are plotted in Fig. 2. The numerical computation always gives a complex eigenvector. For odd $|m|$, the real and imaginary radial profiles coincide with a high numerical accuracy. For even $|m|$, however, as a consequence of the discreteness effect already described above, the radial eigenfunctions of the real and imaginary part differ slightly, especially near the center of the vortex. (Figure 2 only shows a mean value in these cases.) Also, for even $|m|$, the sense of rotation of the eigenmode can only approximately be determined: modes in the continuum theory which belong to positive and negative m intermix in the discrete system for even $|m|$. This second effect is more pronounced for larger $|m|$ and larger system sizes. As a con-
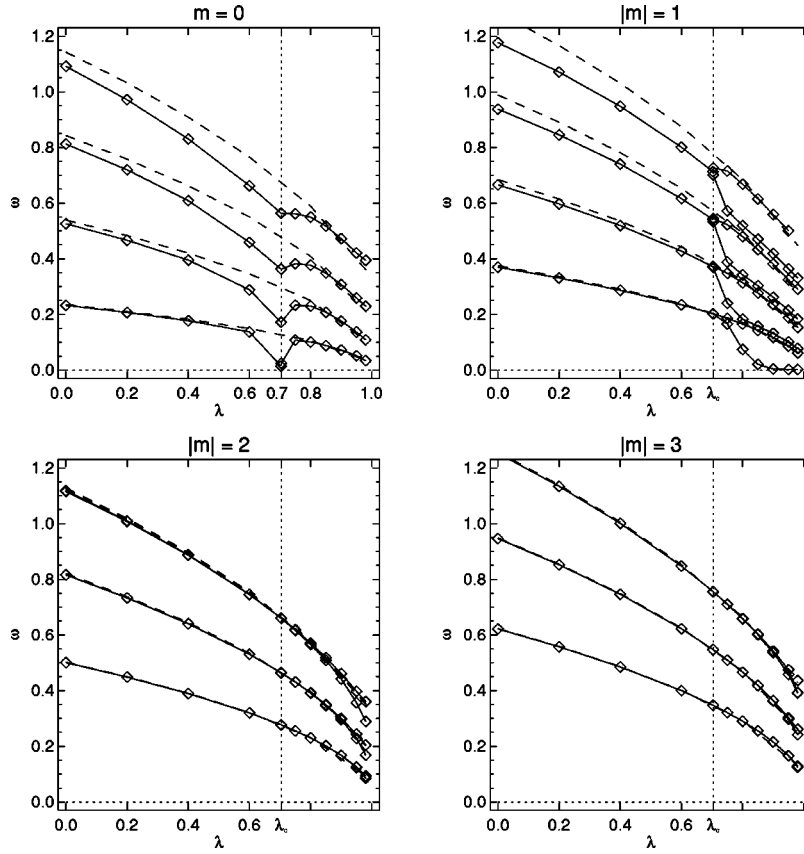
FIG. 1. Eigenvalue spectrum as a function of the anisotropy parameter λ and the ''quantum number of angular momentum'' m calculated for a circular system of radius $L=20$ with fixed boundary conditions. The dashed lines are eigenvalues with no vortex in the system.

sequence, these eigenmodes are not in the separated form of Eqs. (13) and (14).

The main point in our approach is to calculate the scattering matrix $S_m(k)$ and to use its values for the investigation of general properties of the magnon modes in the presence of the vortex. For the extraction of the $S_m(k)$ dependence on the basis of Eqs. (19), (20) we only need values of eigenfrequencies for one boundary condition for different values of the system size. Concretely, we used the fixed BC [$b=0$ in Eq. (19)] leading to the simple formula

$$\sigma_m(k_i) = -\frac{J_m(k_iL)}{Y_m(k_iL)} \tag{28}$$

with $k_i = k_i(\omega_i)$ according to the dispersion law (5).

We calculated the scattering data for four different values of λ, namely, $\lambda = 0.80$, 0.85, 0.90, and 0.98, and for different system sizes up to $L/a_0 = 100$. These data are presented in Fig. 3 as a function of $\kappa = kr_v$. We note that the points $\sigma_m(\kappa)$ fit well to one curve for different L and λ, at least for small values of ka_0. (Strictly speaking, the inequality $ka_0 \ll 1$ should be satisfied, but even for $ka_0 \approx 0.4$ the discrepancies among different values of λ are negligible for the mainly interesting case $|m|=1$.)

For the general boundary conditions (19) the frequency spectrum is determined by the dimensionless equation

$$a[J_m(kL) + \sigma_m(kr_v)Y_m(kL)] + kr_vb[J'_m(kL)$$
$$+ \sigma_m(kr_v)Y'_m(kL)] = 0. \tag{29}$$

We start our discussion for the modes with $|m|>1$ and $m=0$. The translational modes ($|m|=1$) will be considered in the next section.

For $|m|>1$ and fixed BC [$b=0$ in Eq. (19)], taking into account $\sigma_m<0$, it can easily be seen that Eq. (29) has no solution in the region $kL \ll 1$ where $J_m(z) \sim (z/2)^m$ and $Y_m(z) \sim -(2/z)^m/\pi$. The nth root can be written as $kL = z_{n,m}$ with $y_{m,n} < z_{m,n} < j_{m,n}$. Here $y_{m,n}$ and $j_{m,n}$ are the nth zeros of $Y_m(z)$ and $J_m(z)$, respectively. Because $j_{m,n}$ and $y_{m,n}$ are smaller than $\pi(n+m)/2$ for large n or m, the low-lying modes have the values $k_{n,m} \simeq \max(n,m)/L$. This means $\sigma_m \ll 1$ for $r_v/L \ll 1$, hence the eigenfrequencies can approximately be described by the zeros of $J_m(z)$ (which have approximately the same values as for the system without vortex). This can also be observed very clearly in Fig. 1.

For the case $a \sim b$ in the BC (19) the same holds because of the presence of the small parameter kr_v in the term with the derivatives. For $a=0$ (Neumann BC), however, the situation changes. First of all, the formula for $k_{n,m}$ can be presented in the form $k_{n,m} = j'_{m,n}/L$ where $j'_{m,n}$ is the nth zero of $J'_m(z)$. More importantly, a new root of Eq. (29) appears, with $k = k_{0,m} \ll 1/L$ corresponding to the lowest mode with $|m|>1$. In order to show this we use again the asymptotics of $J_m(z)$ and $Y_m(z)$ for $z \ll 1$. Applying the formula $\sigma_m = -A_m(kr_v)^\alpha$, one easily obtains

$$r_vk_{0,m} = \left(\frac{A_m}{\pi}\right)^{p/2m}\left(\frac{2r_v}{L}\right)^p, \quad p = \frac{1}{1-\alpha/2m} > 1. \tag{30}$$
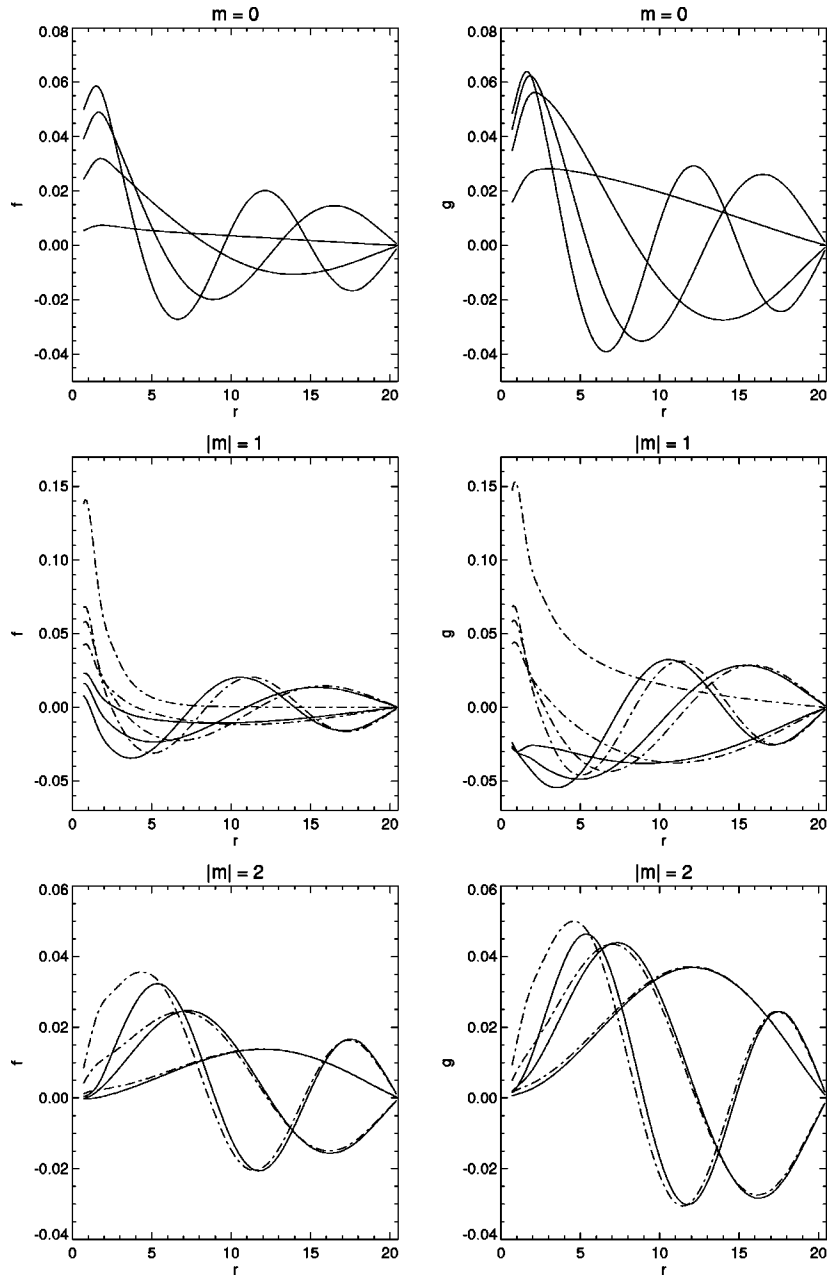
FIG. 2. Radial part of eigenfunctions for the lowest eigenvalues at $\lambda=0.9$ using fixed boundary conditions. Solid and dashed lines correspond to eigenfunctions with positive m and negative m, respectively.

The corresponding frequency $\omega_{0,m}\approx ck_{0,m}$ decreases faster than $1/L$ for $L\rightarrow\infty$.

The eigenmodes with $m=0$ can be described in the same way as for $|m|>1$. Only the values $k_{n,0}=(1/L)j_{0,n}$ or $k_{n,0}=(1/L)j'_{0,n}$ are present in this case, and $k_{n,0}\sim 1/L$ for general boundary conditions. The only exception is the lowest mode for Neumann BC. For this mode the analysis of the asymptotics of cylindrical functions gives exactly $\omega=0$. This value corresponds to the Goldstone mode due to the presence of a rotational symmetry in spin space which is still exact for the finite system.

V. TRANSLATIONAL MODES AND COLLECTIVE VARIABLE APPROACH

This section deals with the analysis of the translational modes $|m|=1$ and the application of their properties for the

construction of equations of motion for the vortex dynamics. From Fig. 3 one can see that the scattering parameter for $|m|=1$ have a linear dependence $\sigma_{\pm 1}(k)=\mp A_1kr_v$. The long-wave approximation (27) gives $A_1=(\pi/4)$, which is in good agreement with Fig. 3. Using the asymptotics $J_1\simeq z/2$, $Y_1\simeq -2/\pi z$ for $z\ll 1$, we get for the frequency of the lowest translational mode $\omega_0=\pm cr_v/L^2$ where the positive sign corresponds to Neumann and the negative sign to Dirichlet boundary conditions, respectively. Using $cr_v=a_0^2JS\sqrt{\lambda}$ and replacing $\sqrt{\lambda}\rightarrow 1$, which is natural in the continuous small anisotropy approximation, we obtain $\omega_0=\pm JSa_0^2/L^2$.

This analytical result is in agreement with the eigenvalue data obtained numerically. However, in the discrete system, ω_0 does actually not tend to zero for $L\rightarrow\infty$ but to a finite constant ω_p. Using the collective variable approach this con-
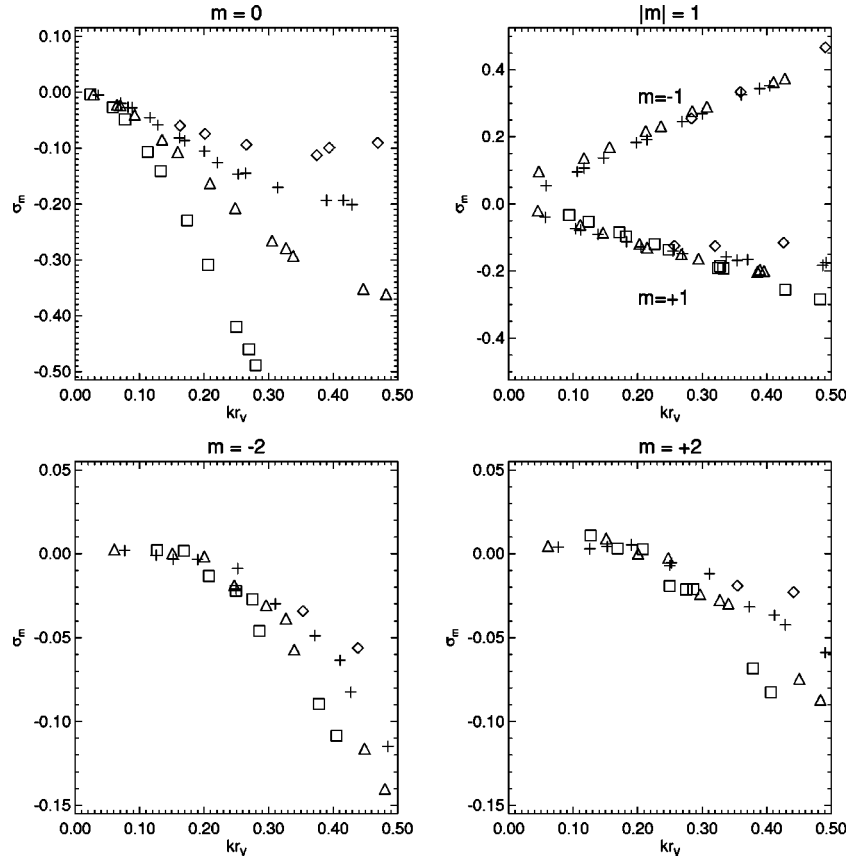
FIG. 3. Scattering data for different values of λ ($\square = 0.80$, $\triangle = 0.85$, $+ = 0.90$, $\diamond = 0.98$) and different system sizes in the range $L = 15$–100.

stant can easily be understood as a pinning effect as we would like to show now. It is known that the dynamics of the OP vortex can be described in lowest approximation by the so-called Thiele equation[18,19]

$$-\vec{G} \times \dot{\vec{X}} = \vec{F}. \tag{31}$$

Here $\vec{G}$ is the gyrovector $\vec{G} = (2\pi qpS/a_0^2)\hat{z}$, where $\hat{z}$ is the unit vector along the hard (z) axis, $\vec{X}$ the position of the vortex center, and $\vec{F}$ the force acting on the vortex. In the case where the vortex is only slightly displaced from the center of the system, Thiele's equation just describes the dynamics of the lowest translational mode. There are two types of forces acting on the vortex. The first one is due to an image vortex which resides at the position $(L^2/X^2)\vec{X}$, $X = |\vec{X}|$, and the second one is due to the pinning potential of the underlying lattice. Putting both together we obtain

$$-\vec{G} \times \dot{\vec{X}} = -\frac{2\pi JS^2 qq_i \vec{X}}{L^2 - X^2} - k_p\vec{X}, \tag{32}$$

where q_i is the vorticity of the image vortex. We have assumed that the pinning potential is harmonic in lowest approximation leading to a linear force with spring constant k_p. In the limit $X \to 0$, Eq. (32) has the solution $X_1(t) = X \cos \omega_0 t$, $X_2(t) = X \sin \omega_0 t$ with

$$\omega_0 = -\frac{qq_i JSa_0^2}{L^2} - \frac{k_p a_0^2}{2\pi S} \tag{33}$$

which, apart from the constant part, agrees with the dependency we have found above. In order to calculate k_p from the numerical eigenvalue data one can use the fact that Dirichlet boundary conditions generate an image of the same vorticity while Neumann boundary conditions generate an image of opposite vorticity. Therefore from Eq. (33) two equations follow:

$$\omega_{0,\text{Dirichlet}} = -\frac{JSa_0^2}{L^2} - \frac{k_p a_0^2}{2\pi S},$$

$$\omega_{0,\text{Neumann}} = +\frac{JSa_0^2}{L^2} - \frac{k_p a_0^2}{2\pi S}. \tag{34}$$

Adding them leads to the following formula for ω_p which is independent of the concrete size of the system:

$$\omega_p \equiv -\frac{k_p a_0^2}{2\pi S} = \frac{\omega_{0,\text{Dirichlet}} + \omega_{0,\text{Neumann}}}{2}. \tag{35}$$

Assuming a pinning potential of the form $E_p[\cos(2\pi x/a_0) + \cos(2\pi y/a_0) + 2]/2$, ω_p is connected to the pinning energy E_p by the formula

$$E_p = \frac{S|\omega_p|}{\pi}. \tag{36}$$

We have evaluated Eqs. (35) and (36) for some values of λ, see Table I. Naturally, the pinning energy decreases with

TABLE I. Pinning frequency and energy in dependence of the anisotropy paramter λ.

λ	$|\omega_p|/JS$	$E_p/(JS^2)$	$E_p^{\text{direct}}/(JS^2)$
0.80	0.0672	0.0214	0.0233
0.85	0.0181	5.76×10^{-3}	5.87×10^{-3}
0.90	1.88×10^{-3}	5.98×10^{-4}	6.05×10^{-4}
0.98	8.07×10^{-5}	2.57×10^{-5}	3.85×10^{-6}

decreasing anisotropy because the size of the OP structure increases strongly, making discreteness effects less and less important.

The pinning energy can also be measured directly, comparing the energy of static vortices centered on different lattice coordinates. These numbers, labeled E_p^{direct} in Table I, compare very well with E_p due to formula (36).

Next, we discuss the higher modes obeying the $|m|=1$ symmetry. Due to the general features discussed in the previous section, these modes can be considered as doublets, with frequencies $\omega_n > 0$ and $\omega_{n+1} < 0$ with $|\omega_{n+1}| \simeq \omega_n$. For general BC's the mean frequency can be written as

$$\bar{\omega}_n \simeq c x_n / L, \tag{37}$$

where x_n is the nth root of the equation $a J_1(x) + b x (r_v/L) J_1'(x) = 0$. For fixed and free BC's one has $\bar{\omega}_n = c j_{1,n}/L$ and $\bar{\omega}_n = c j_{1,n}'/L$, respectively.

We concentrate on the lowest doublet with the frequencies ω_1 and $\omega_2 \simeq -\omega_1$ for the following reasons: (i) these modes can be compared with long-time computer simulations of the vortex motion and (ii) they can be used for the calculation of parameters in equations of the vortex motion. In the lowest approximation in r_v/L one can write

$$\frac{\bar{\omega}_1}{SJ} \simeq 2 x_1 \sqrt{1-\lambda} \frac{a_0}{L}, \tag{38}$$

where $x_1 = j_{1,1} \simeq 3.832$ for fixed BC's and $x_1 \simeq j_{1,1}' \simeq 1.8412$ for free ones. For general BC's x_1 lies between these values. Note, however, that for $a \approx b$ the value of x_1 is still close to $j_{1,1}$, and the ''switching'' to the value $j_{1,1}'$ occurs only for small $a \lesssim b(a_0/L)$. We remind the reader that $\bar{\omega}_1$ does not depend on the scattering data in the first approximation in a_0/L. The use of scattering data becomes important, however, for the calculation of the doublet width $\Delta \omega = |\omega_2| - \omega_1$. Considering the leading approximation $k r_v \sim a_0/L$, the width can be presented in the form

$$\frac{\Delta \omega}{SJ} = \frac{\pi \sqrt{\lambda}}{2} \left(\frac{a_0}{L} \right)^2 \frac{x_1^2 (a x_1 - b) Y_1 + x_1 b Y_0}{x_1 (x_1 a - b) J_0 + [(2 - x_1^2) b - x_1 a] J_1}, \tag{39}$$

where J_0, J_1, Y_0, and Y_1 all have the argument x_1. One can see that $\Delta \omega$ is practically independent of the anisotropy (we will omit the coefficient $\sqrt{\lambda}$ below), and it is inversely proportional to L^2. This is the same dependence as for the lowest translational mode $\omega_0 \simeq JS(a_0/L)^2$, but the coefficients are different.

Next we compare our results for ω_0 and the lowest doublet $\omega_{1,2}$ with data from recent computer simulations[17] for
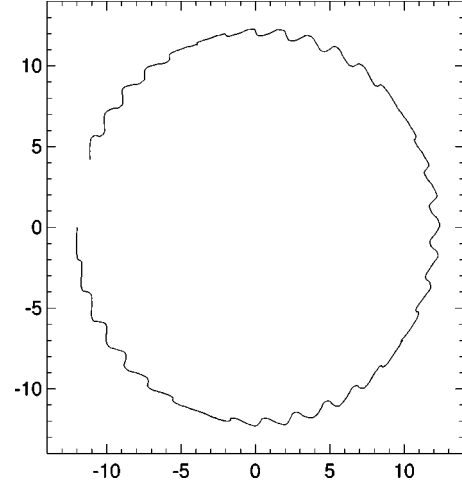

FIG. 4. Trajectory of a vortex obtained by numerically integrating the Landau Lifshitz equation in time. The simulation was performed on a circular system with radius $L = 36 a_0$ and free boundary conditions.

the motion of one OP vortex on large circular systems (up to $L = 72 a_0$) with free boundaries. The Landau-Lifshitz equation was integrated for a square lattice with $a_0 = 1$ and the Hamiltonian (1), where $J = S = 1$ and $\lambda = 0.9$. The vortex center performs oscillations around a mean trajectory $\vec{X}^0(t)$ which is a circle with radius R_0 around the circle center (Fig. 4). The mean trajectory can be interpreted as a stationary solution of the Thiele equation (31), where the vortex is driven by the interaction with its image vortex. The rotational frequency ω_0 goes to a constant for $R_0 \to 0$; the extrapolated value 0.201×10^{-3} agrees well with our result 0.193×10^{-3} (both for $L = 72$).

The Fourier spectrum of the oscillations around $\vec{X}^0(t)$ shows a doublet $\omega_{1,2}'$ with about equal amplitudes, and phases $\mp \pi/2$ between the two components. As the spectra in Ref. 17 were evaluated in a moving polar coordinate frame we must add and subtract ω_0 in order to compare with our results in Eqs. (38) and (39)

$$\omega_{1,2} = \omega_{1,2}' \pm \omega_0. \tag{40}$$

The data agree very well, e.g., for $L = 72$ and $R_0 = 16.11$ the frequencies $\omega_0 = 2.05 \times 10^{-4}$, $\omega_1' = 1.546 \times 10^{-2}$, and $\omega_2' = 1.661 \times 10^{-2}$ were observed which yields $\bar{\omega} = 1.604 \times 10^{-2}$ for the mean and $\Delta \omega = 0.74 \times 10^{-3}$ for the difference. This agrees with our theoretical values $\bar{\omega} = 1.617 \times 10^{-2}$ and $\Delta \omega = 0.7657 \times 10^{-3}$ within 0.8 and 4 %, respectively.

Note that the very good agreement of our normal mode approach with the data from the simulations is not a trivial result: we have calculated the frequencies appearing in the vortex dynamics for *free boundary conditions*, using as input the scattering data for *fixed boundary conditions*. This shows that our scattering theory actually works for the general case.

We conclude that the vortex motion is accompanied by, or generates, the two quasilocal magnon modes with $|m|=1$. These show up in two ways: (i) in the trajectory of the vortex

center as oscillations around a mean trajectory, (ii) as oscillations of the dynamic parts of the vortex structure (see below).

There remains the question of whether the trajectory of the vortex center can be obtained from an equation of motion. If the rigid-shape assumption of Thiele is dropped by allowing for a deformation due to the velocity,[21] a second-order equation of motion can be derived[22] which exhibits an additional term $M\ddot{\vec{X}}$ with an effective vortex mass M. The additional term causes cycloidal oscillations[23] with frequency $\omega_c = G/M$ around a mean trajectory. For the vortex mass $M \sim \ln L$ was predicted, which was not confirmed by computer simulations, see Refs. 24, 25. Recently Wysin[16] proposed to calculate M by using the two lowest eigenfrequencies, ω_0 and ω_1 in our notation. His formula $M_W = G/(\omega_0 + \omega_1)$ gave a linear L dependence when the frequencies from his numerical diagonalization were inserted. The same dependence is obtained [in $O(a_0/L)$] if we insert our analytical results for the frequencies.

However, meanwhile new simulations had been performed which resulted in the observation of the abovementioned doublet $\omega_{1,2}$, instead of a single frequency ω_c. This dynamics can be fully described by a third-order equation of motion[17] which was derived by a collective variable theory, starting from a generalized traveling wave ansatz

$$\vec{S}(\vec{r},t) = \vec{S}(\vec{r} - \vec{X}, \dot{\vec{X}}, \ddot{\vec{X}}), \tag{41}$$

where the vortex shape is assumed to depend also on the acceleration. In fact, this dependence can be seen in simulations with free BC's when one considers the spin configurations at the turning points of the trajectory where the acceleration is maximum while the velocity is small.[17]

The third-order equation has the form

$$\vec{G}_3 \times \dddot{\vec{X}} + M\ddot{\vec{X}} - \vec{G} \times \dot{\vec{X}} = \vec{F} \tag{42}$$

with $\vec{G}_3 = G_3 \vec{e}_z$ and a new parameter G_3. We note that this is the most general third-order equation for the given easy-plane symmetry. In Ref. 17, G_3 was defined as an integral over $\vec{r}$ which could not be performed because the dynamic vortex structure is not known analytically for the vortex core. However, the size dependence $G_3 \sim L^2$ was obtained from the outer region of the integral. We will see below that our theory allows for the calculation of G_3 and M.

We consider Eq. (42) for the case of vortex motion close to the center of the circle where the image force is approximately linear

$$\vec{F} = -2\pi q q_i \vec{X}/L^2. \tag{43}$$

Then Eq. (42) can be solved by a harmonic ansatz, where the frequency ω fulfills

$$-G_3\omega^3 - M\omega^2 + G\omega = -2\pi q q_i/L^2. \tag{44}$$

The parameters can be obtained from the three roots ω_i, using Vieta's rules

$$\omega_0 + \omega_1 + \omega_2 = -M/G_3, \tag{45}$$

$$\omega_0\omega_1 + \omega_0\omega_2 + \omega_1\omega_2 = -G/G_3, \tag{46}$$

$$\omega_0\omega_1\omega_2 = 2\pi q q_i/(G_3 L^2). \tag{47}$$

We now identify ω_0 with the Goldstone mode $-q q_i/L^2$, neglecting the frequency ω_p from the pinning force since Eq. (42) was derived in the continuum limit; ω_1 and $\omega_2 < 0$ are identified with the lowest doublet calculated in Eqs. (38), (39).

From Eq. (47) we obtain[26]

$$G_3 = \frac{2\pi}{\bar{\omega}^2} \tag{48}$$

with $\bar{\omega} = \sqrt{|\omega_1\omega_2|} \simeq \frac{1}{2}(\omega_1 + |\omega_2|)$, which gives

$$G_3 = \frac{\pi}{2x_1^2(1-\lambda)}L^2. \tag{49}$$

The result $4.634 \, L^2$ for free BC's agrees very well with $4.67 \, L^{2.002}$ for large L obtained from the simulation data.[17] For fixed BC's, $G_3 = 1.07 \, L^2$ is about four times smaller.

From Eq. (45) we obtain

$$M = \frac{2\pi}{\bar{\omega}^2}\left(\Delta\omega + \frac{q q_i}{L^2}\right) \tag{50}$$

with $\Delta\omega = |\omega_2| - \omega_1$. Here all L dependencies just cancel in the lowest approximation on L, thus the vortex mass in Eq. (42) is *independent* of the system size, as already obtained from the simulations.[17] Inserting Eq. (39) we get for free BC's

$$M = \frac{\pi}{2(1-\lambda)}\left(\frac{\pi}{2}\frac{x_1 Y_0 - Y_1}{(x_1^2 - 1)J_1} - \frac{1}{x_1^2}\right). \tag{51}$$

The numerical value $M = 14.74$ agrees well with $M = 15$ which we have extrapolated for $R_0 \to 0$ from the data in Ref. 17 for three different system sizes ($L = 24, 36, 72$). We note that the vortex mass (51) is in the same order of magnitude as the two-dimensional soliton mass $M = E_0/c^2$ in Ref. 21, where $E_0 = 4\pi$ (in units JS^2) is the Belavin-Polyakov energy.

For fixed BC's

$$M = \frac{\pi}{2(1-\lambda)}\left(\frac{\pi}{2}\frac{Y_1}{x_1 J_0} + \frac{1}{x_1^2}\right) \tag{52}$$

yields $M = 7.661$, which is about one half of the above value for free boundary condition. Thus in the equation of motion (42) only the gyrovector $\vec{G}$ is an intrinsic property of the vortex. The quantities M and G_3, which are connected to the quasilocal modes with frequencies $\omega_{1,2}$, are determined by the whole system ''vortex plus magnons'' which includes the geometry of the system and the boundary conditions. For G_3 this is obvious because it strongly depends on L; but M does not depend on L (in the lowest order), however, it depends on the boundary conditions. On the other hand, the S matrix naturally is determined only by the region of the vortex core and can thus be used for the calculation of the parameters M and G_3 for arbitrary geometry and boundary conditions.

Finally we point out that Eq. (42) belongs to a whole hierarchy of equations of motion which can be derived[17] by

taking into account higher and higher time derivatives of $\vec{X}(t)$ in the generalized traveling wave ansatz (41). Moreover, only the odd-order equations of this hierarchy represent valid approximations, because the even-order equations have a very weak leading term, e.g., $M\ddot{\vec{X}}$ in the second-order equation. Therefore the solutions of the latter equations are qualitatively different from the solutions of the odd-order equation and are in fact not confirmed by the simulations (see the above discussion of the single frequency ω_c and the doublet $\omega_{1,2}$, which exhibit quite different dependencies on the system size). The fifth-order equation of the hierarchy predicts a second doublet $\omega_{3,4}$ which was in fact observed in the simulations, but only for specially designed initial and boundary conditions because the amplitudes of this doublet are very small.[17] Thus the third-order equation represents already a very good approximation. The observed additional doublet naturally also appears in the results of our numerical diagonalization in Sec. IV and its frequencies can be calculated by $\bar{\omega}_n$ and $(\Delta\omega)_n$, see Eq. (37) and below.

VI. CONCLUSION

We have developed a general theory which allows calculation of the magnon modes of a circular easy-plane ferromagnet in the presence of an out-of-plane vortex. The method consists of a combination of numerical diagonalization of the discrete system with analytical calculations in the continuum limit. The frequencies of the magnon modes can be expressed in terms of the functions $\sigma_m(kr_v)$, which are independent of the magnetic coupling constants, the system size, and the boundary conditions. The σ_m describe the intensity of the magnon scattering due to the presence of the vortex.

The translational modes with $|m|=1$ are particularly interesting for two reasons: (i) Their frequencies are identified in the vortex motion which was observed in simulations where the Landau-Lifshitz equation was integrated for the circular discrete spin system. (ii) Using these frequencies, one can calculate the two parameters of a third-order equation for the vortex motion (a generalization of the Thiele equation), which was derived by a collective variable theory starting from a generalized traveling wave ansatz. Our calculated parameters agree very well with those obtained by describing the simulations using the third-order equation of motion. Both parameters, the vortex mass M and the third-order gyrocoupling constant G_3, depend strongly on the boundary conditions. This is due to the fact that both the in-plane and the out-of-plane structure of the moving vortex are not localized. In fact, the dynamic parts of the vortex structure oscillate with the frequencies of the translational modes with $|m|=1$.

ACKNOWLEDGMENTS

APPENDIX: NUMERICAL DIAGONALIZATION OF HAMILTONIAN MATRICES

If a classical Hamiltonian system is linearized around a static solution, an eigenvalue problem

$$\mathbf{A}\vec{z}=\lambda\vec{z} \tag{A1}$$

results with a coefficient matrix $\mathbf{A}$ fulfilling the generalized symmetry relation

$$\mathbf{A}^T\mathbf{J}=\mathbf{J}^T\mathbf{A}. \tag{A2}$$

$\mathbf{J}$ is the "symplectic unit matrix," i.e.,

$$\mathbf{J}=\begin{pmatrix} \mathbf{0} & \mathbf{1} \\ -\mathbf{1} & \mathbf{0} \end{pmatrix}. \tag{A3}$$

For obvious reasons the matrix $\mathbf{A}$ is called a "Hamiltonian matrix." It is easy to see that $\mathbf{A}$ can always be written as $\mathbf{JH}$ where $\mathbf{H}$ is a symmetric matrix. Note that the eigenvalues and eigenvectors of $\mathbf{A}$ are complex in general.

For the most general case, Hamiltonian matrices have no special properties which could profitably be used in the numerical diagonalization. An exception, however, is the case of a positive definite matrix $\mathbf{H}$, for which Eq. (A1) is equivalent to an Hermitian eigenvalue problem with pure imaginary eigenvalues. In order to show this, we note that a positive definite matrix can always be written as

$$\mathbf{H}=\mathbf{L}\mathbf{L}^T, \tag{A4}$$

the so-called Cholesky decomposition of $\mathbf{H}$, cf. Ref. 27. Substituting this in Eq. (A1) and additionally defining $\lambda:=i\omega$ we obtain

$$(i\mathbf{L}^T\mathbf{J}\mathbf{L})(\mathbf{L}^T\vec{z})=-\omega(\mathbf{L}^T\vec{z}). \tag{A5}$$

Now, $\mathbf{J}$ is antisymmetric and therefore $i\mathbf{L}^T\mathbf{J}\mathbf{L}$ is Hermitian.

Unfortunately, it is somewhat difficult to use this equivalence directly for the purpose of numerical diagonalization. The Cholesky decomposition of a sparse symmetric matrix can be computed easily only for certain cases, otherwise it is very time consuming. For this reason we did not directly use formula (A4). Instead we utilized a method called Wielandt's version of the inverse iteration procedure. The basic strategy is to multiply a (randomly chosen) vector over and over by the inverse of the spectral-shifted matrix $\mathbf{A}$, i.e., $(\mathbf{A}-\bar{\lambda}\mathbf{I})^{-1}$. The resulting series of vectors converges to an eigenvector of $\mathbf{A}$, usually the one corresponding to the eigenvalue closest to the chosen spectral shift $\bar{\lambda}$. The details of the method can be found in Ref. 27. For Hamiltonian matrices, supposing a positive definite matrix $\mathbf{H}$ and therefore imaginary eigenvalues and an imaginary spectral shift $\bar{\lambda}=i\bar{\omega}$, Wielandt's inverse iteration amounts to the following iteration formula:

$$\begin{pmatrix} \mathbf{H} & -\bar{\omega}\mathbf{J} \\ \bar{\omega}\mathbf{J} & \mathbf{H} \end{pmatrix}\begin{pmatrix} \vec{x}^{(j+1)} \\ \vec{y}^{(j+1)} \end{pmatrix}=-\begin{pmatrix} \mathbf{J}\mathcal{P}\vec{x}^{(j)} \\ \mathbf{J}\mathcal{P}\vec{y}^{(j)} \end{pmatrix}. \tag{A6}$$

$\vec{x}^{(j)}$ and $\vec{y}^{(j)}$ are the real and imaginary part of the eigenvector in the jth iteration step. The initial vector $(\vec{x}^{(0)}, \vec{y}^{(0)})$ must be chosen randomly. The matrix $\mathcal{P}$ is a symplectic projection operator which is defined as

$$\mathcal{P} = \sum_{k \leq j} \frac{\vec{y}^{(k)} \vec{x}^{(k)T} - \vec{x}^{(k)} \vec{y}^{(k)T}}{\vec{x}^{(k)T} \mathbf{J} \vec{y}^{(k)}} \mathbf{J}. \tag{A7}$$

The sum runs over all eigenvectors which were computed in previous runs. The purpose of this operator is to avoid that the method converges to an already-known eigenvector.

After some iteration steps the parameter $\bar{\omega}$ can also be iterated, for example, according to the formula

$$\bar{\omega} = \frac{1}{i} \frac{\vec{z}^{+} \mathbf{A} \vec{z}}{|\vec{z}|^2}, \quad \vec{z} = \vec{x}^{(j)} + i \vec{y}^{(j)}. \tag{A8}$$

As $\vec{z}$ converges to an eigenvector of $\mathbf{A}$, $\bar{\lambda}$ converges to the corresponding eigenvalue.

A positive definite matrix $\mathbf{H}$ is not a principal presumption for the inverse iteration, i.e., the above iteration formula can in principle be generalized to include the case of nondefinite matrices $\mathbf{H}$. However, first of all, with $\mathbf{H}$, the coefficient matrix in Eq. (A6) is also positive definite. This allows us to use an efficient numerical method to solve Eq. (A6). To be precise we have used the NAG library function F04MBF for this purpose which is based on a Lanczos algorithm. The NAG routine makes it only necessary to supply a ''matrix$\times$vector'' function. Therefore one has to store only the elements of $\mathbf{A}$ which are nonzero which precisely makes the method suitable for large and sparse matrix equation. A second point is that for nondefinite $\mathbf{H}$ rather serious problems with the numerical stability of the inverse iteration arise.

---

*Permanent address: Institute for Metal Physics, Ukraine Academy of Sciences, 36, Vernadskii St., Kiev 252142, Ukraine.

[1] A. M. Kosevich, B. A. Ivanov, and A. S. Kovalev, Phys. Rep. **194**, 117 (1990).

[2] V. G. Bar'yakhtar and B. A. Ivanov, in Sov. Sci. Rev., Sect. A **16**, 3 (1993).

[3] B. A. Ivanov and A. K. Kolezhuk, Low Temp. Phys. **21**, 275 (1995).

[4] A. P. Malozemoff and J. C. Slonczewski, *Magnetic Domain Walls in Bubble Materials*, Applied Solid State Science, Supplement I (Academic, New York, 1979).

[5] F. G. Mertens, A. R. Bishop, G. M. Wysin, and C. Kawabata, Phys. Rev. Lett. **59**, 117 (1987); Phys. Rev. B **39**, 591 (1989).

[6] H.-J. Mikeska and M. Steiner, Adv. Phys. **40**, 191 (1991).

[7] J. M. Kosterlitz and D. J. Thouless, J. Phys. C **6**, 1181 (1973).

[8] J. M. Kosterlitz, J. Phys. C **7**, 1046 (1974).

[9] V. L. Berezinskii, Sov. Phys. JETP **32**, 493 (1970); **34**, 610 (1972).

[10] E. G. Galkina and B. A. Ivanov, JETP **82**, 1168 (1996).

[11] G. M. Wysin, Phys. Rev. B **49**, 8780 (1994).

[12] G. M. Wysin and A. R. Völkel, Phys. Rev. B **52**, 7412 (1995); **54**, 12 921 (1996).

[13] B. A. Ivanov, A. K. Kolezhuk, and G. M. Wysin, Phys. Rev. Lett. **76**, 511 (1996).

[14] B. V. Costa, M. E. Gouvêa, and A. S. T. Pires, Phys. Lett. A **156**, 179 (1992).

[15] A. R. Pereira, F. O. Coelho, and A. S. T. Pires, Phys. Rev. B **54**, 6084 (1996).

[16] G. M. Wysin, Phys. Rev. B **54**, 15 156 (1996).

[17] F. G. Mertens, H. J. Schnitzer, and A. R. Bishop, Phys. Rev. B **56**, 2510 (1997).

[18] A. A. Thiele, Phys. Rev. Lett. **30**, 230 (1973); J. Appl. Phys. **45**, 377 (1974).

[19] D. L. Huber, Phys. Rev. B **26**, 3758 (1982).

[20] H. J. Schnitzer, Ph. D. thesis (in German), University of Bayreuth, 1996.

[21] A mass, due to a velocity induced shape deformation, was already introduced for the solitons in 2D easy-axis ferromagnets, see B. A. Ivanov and V. A. Stephanovich, Phys. Lett. A **141**, 89 (1989).

[22] G. M. Wysin and F. G. Mertens, in *Nonlinear Coherent Structures in Physics and Biology*, edited by M. Remoissenet and M. Peyrard, Vol. 393 of Springer Lecture Notes in Physics (Springer, Berlin, 1991); G. M. Wysin, F. G. Mertens, A. R. Völkel, and A. R. Bishop, in *Nonlinear Coherent Structures in Physics and Biology*, edited by K. H. Spatschek and F. G. Mertens (Plenum, New York, 1994).

[23] These trajectories correspond to the cycloids with frequency $eB/(Mc)$ of an electric charge e in a plane with a perpendicular magnetic field $\vec{B}$ and an in-plane electric field $\vec{E}$, where c is the speed of light.

[24] F. G. Mertens, G. M. Wysin, A. R. Völkel, A. R. Bishop, and H. J. Schnitzer, in *Nonlinear Coherent Structures in Physics and Biology* (Ref. 22).

[25] A. R. Völkel, G. M. Wysin, F. G. Mertens, A. R. Bishop, and H. J. Schnitzer, Phys. Rev. B **50**, 12 711 (1994).

[26] Equation (46) gives the same result, because a term $\omega_0 \Delta \omega / \bar{\omega}^4$ can be neglected.

[27] J. Stoer and R. Bulirsch, *Introduction to Numerical Analysis* (Springer, Berlin, 1993).